FULL PAPER

ADVANCED
FUNCTIONA
MATERIALS
www.afm-journal.d

Check for updates

Constructing Na-Ion Cathodes via Alkali-Site Substitution

Chenglong Zhao, Zhenpeng Yao, Dong Zhou, Liwei Jiang, Jianlin Wang, Vadim Murzin, Yaxiang Lu,* Xuedong Bai, Alán Aspuru-Guzik, Liquan Chen, and Yong-Sheng Hu*

Na-ion batteries have experienced rapid development over the past decade and received significant attention from the academic and industrial communities. Although a large amount of effort has been made on material innovations, accessible design strategies on peculiar structural chemistry remain elusive. An approach to in situ construction of new Na-based cathode materials by substitution in alkali sites is proposed to realize long-term cycling stability and high-energy density in low-cost Na-ion cathodes. A new compound, $[K_{0.444(1)}Na_{1.414(1)}][Mn_{3/4}Fe_{5/4}](CN)_6$, is obtained through a rational control of K^+ content from electrochemical reaction. Results demonstrate that the remaining K^+ (≈ 0.444 mol per unit) in the host matrix can stabilize the intrinsic K-based structure during reversible Na^+ extraction/insertion process without the structural evolution to the Na-based structure after cycles. Thereby, the as-prepared cathode shows the remarkably enhanced structural stability with the capacity retention of >78% after 1800 cycles, and a higher average operation voltage of ≈ 3.65 V versus Na^+/Na, directly contrasting the non-alkali-site-substitution cathode materials. This provides new insights into alkali-site-substitution constructing advanced Na-ion cathode materials.

1. Introduction

Recently, Na-ion batteries (NIBs) have been considered a promising supplement to Li-ion batteries (LIBs) in smart grids and efficient grid-scale applications owing to the abundance of Na resources.[1] However, compared to highly commercial LIBs technology, there are still several challenges holding back the large-scale applications of NIBs, which is due to a lack of high-performance cathode materials.[2] The large atomic mass and relatively high redox potential (–2.71 V vs standard hydrogen electrode) of Na essentially limit their energy density. In addition, searching for the suitable cathode materials with superior cycling life is of great importance for the practical applications.

Up to now, cathode materials in different crystal structures have been investigated the Na storage performance,[3] including oxides,[4] polyanionic compounds,[5] Na super ionic conductors,[6] and organic compounds.[7] As for the reported cathode materials, a general formula, [A][TM][AG], can be proposed to describe the compositional and structure configurations for a simple classification. [A] denotes the Na^+ sites in a crystal structural. [TM] is the transition metal sites, which can be occupied by one or multiple TM elements having identical oxidation states or a mixture of different valence-state elements. [AG] represents the sites of anions or anion groups. Generally, the performance of cathode materials can be improved by the substitution of various compositions and/or proportions of the two parts of [TM] and [AG] in a same structure type. For example, by substituting Ni^{2+} with inactive Mg^{2+} in $Na_{0.67}[Mn_{0.67}Ni_{0.23}Mg_{0.1}]O_2$, the undesired phase transition was reduced to some content, leading to an enhanced capacity retention.[8] Through the introduction of the TM vacancy

C. Zhao, L. Jiang, Dr. Y. Lu, Prof. L. Chen, Prof. Y.-S. Hu
Key Laboratory for Renewable Energy
Beijing Key Laboratory for New Energy Materials and Devices
Beijing National Laboratory for Condensed Matter Physics
Institute of Physics
Chinese Academy of Sciences
Beijing 100190, China
E-mail: yxlu@aphy.iphy.ac.cn; yshu@aphy.iphy.ac.cn

C. Zhao, L. Jiang, Dr. Y. Lu, Prof. Y.-S. Hu
Center of Materials Science and Optoelectronics Engineering
University of Chinese Academy of Sciences
Beijing 100049, China

Dr. Z. Yao, Prof. A. Aspuru-Guzik
Department of Chemistry and Chemical Biology
Harvard University
Cambridge, MA 02138, USA

Dr. D. Zhou
Helmholtz Zentrum Berlin für Materialien und Energie
Hahn-Meitner-Platz 1, 14109 Berlin, Germany

J. Wang, Prof. X. Bai
State Key Laboratory for Surface Physics
Institute of Physics
Chinese Academy of Sciences
Beijing 100190, China

Dr. V. Murzin
Bergische Universität Wuppertal
Gaußstraße 20, 42119 Wuppertal, Germany

Prof. A. Aspuru-Guzik
Department of Chemistry and Department of Computer Science
University of Toronto
Toronto, ON M5S 3H6, Canada

Prof. Y.-S. Hu
Yangtze River Delta Physics Research Center Co. Ltd.
Liyang 213300, China

($\square_{TM}$) in $Na_x[TM\square_{TM}]O_2$, the oxygen redox activity was successfully triggered toward a higher capacity.[9] Furthermore, with regard to [AG], a new $NaFe_2PO_4(SO_4)_2$ cathode was reported by the substitution of PO_4^{3-} to SO_4^{2-} in $Fe_2(SO_4)_3$ structural model, as well by introducing Na^+ to balance the total charge.[10] The obtained low-cost material exhibited a single-phase reaction having a capacity of ≈100 mAh g^{-1} after 50 cycles. By comparison, the substitution and/or doping in [A] sites have received less research attention. Although several reports claimed that the [A]-site substitution can be prepared directly by the conventionally chemical synthesis,[11] there are several potential issues that should be further taken into accounts for the case of [A] sites: 1) the selection of substituted/doped ions; 2) the concentration/proportion of these ions; and 3) the control of these ions into the pristine

[A] sites. Usually, the amount of these alien ions should be less in the [A] sites because the excess would block the migration of [A] ions and decrease the total capacity as well as destroy the pristine structure, the attention to which has not been paid.

In this work, we introduce an approach to design new [A]-site-substituted Na-ion cathodes via electrochemical extraction/insertion reaction based on the rational selection and control of alien ions, as illustrated in **Figure 1**a. Generally, as for the single A-containing electrode materials, in which A is the ions in [A] sites for extraction/insertion during the electrochemical process, whose electrochemical properties, including structural stability, operation voltage, and capacity, highly depend on the structural and chemical natures of A^{n+}. If we want to use B^{n+} as the alien ions to improve the structural
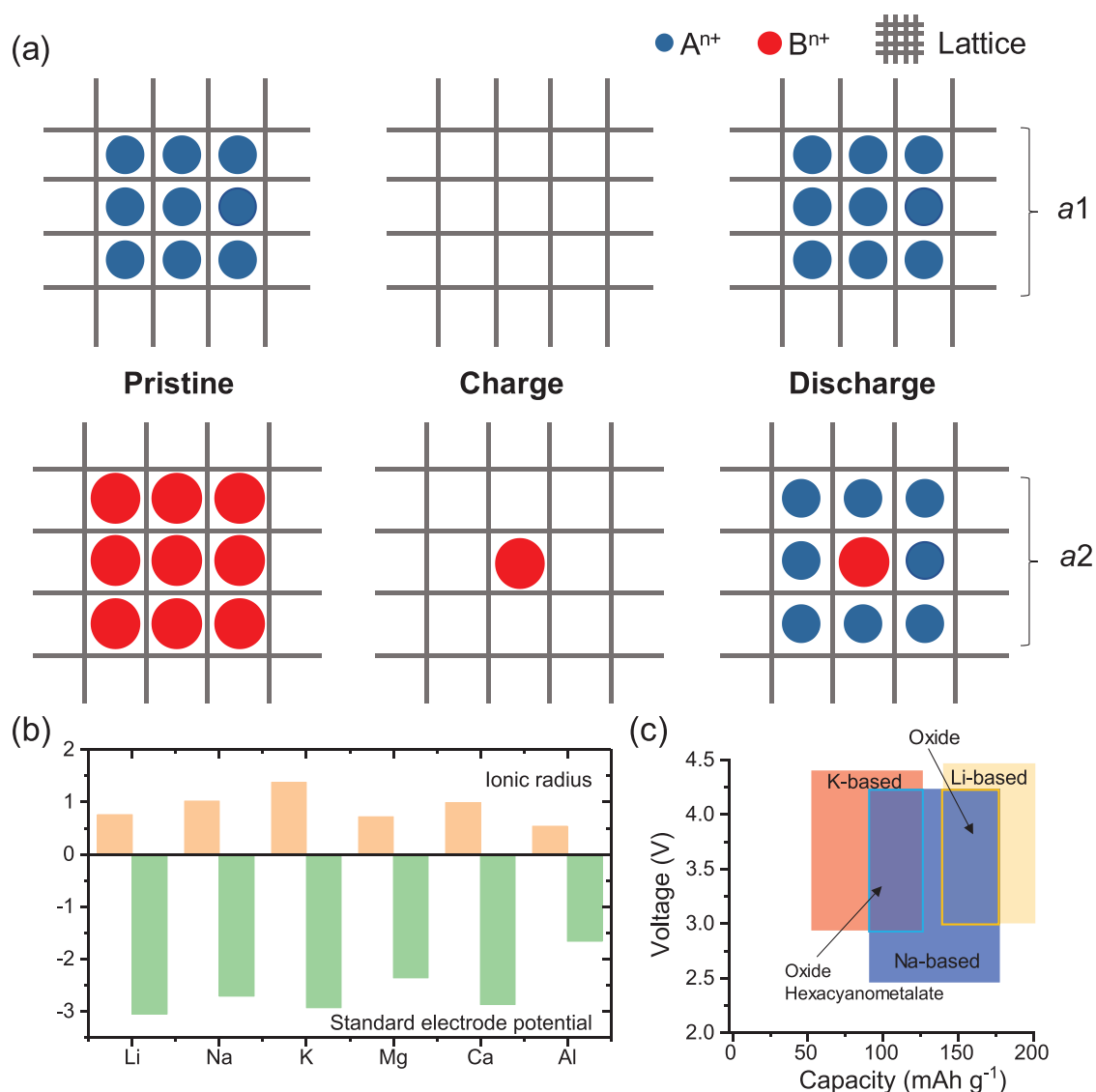
Figure 1. Proposed mechanism of in situ-formed [A]-substituted cathodes for rechargeable batteries. a) Schematic illustration of the general batteries operated with the same ions and the current batteries operated with the different ions. These cathodes can be obtained from the electrochemical reaction, by using A-containing compound as an electrode, B-containing salt as electrolyte and B-containing compound as counter electrode. b) Ionic radius and electrode potential (vs standard hydrogen electrode) of the current ion's secondary batteries. c) Capacity versus voltage of reported cathodes.
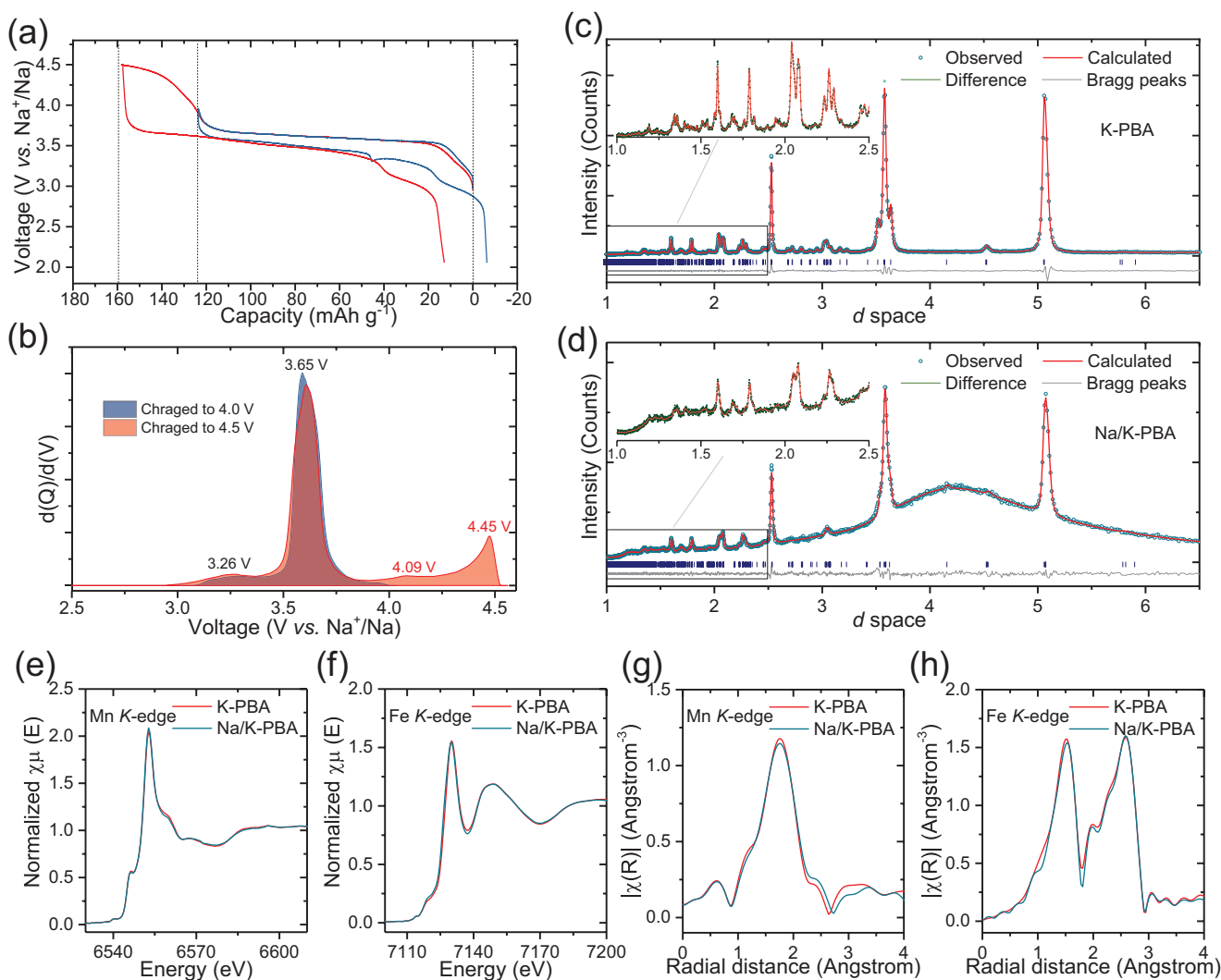
Figure 2. Structural characterization on the as-prepared cathodes. a) Charge–discharge curves of the $K_{1.789}[Mn_{3/4}Fe_{5/4}](CN)_6$ cathode in Na-based electrolyte with Na metal as anode cycled at a current density of 10 mA g^{-1} in the voltage range of 2.0–4.5 V and 2.0–4.0 V. b) d(Q)/d(V) plots of the charge curves in different voltage ranges. Rietveld refinement of XRD patterns of $K_{1.789}[Mn_{3/4}Fe_{5/4}](CN)_6$ cathode c) in the pristine state and d) after one cycle in the voltage range of 2.0–4.0 V ($[K_{0.444(1)}Na_{1.414(1)}][Mn_{3/4}Fe_{5/4}](CN)_6$). XANES spectra of the e) Mn K-edge and f) Fe K-edge in the pristine state and after one cycle in the voltage range of 2.0–4.0 V. f,g) EXAFS spectra of the samples at different states.

stability of A-containing electrode materials, it is first recommended to select the bigger substituted/doped ions to serve as the "pillar" in pristine structure, in which these bigger B^{n+} can provide the corresponding larger cell volume or lattice parameters (according to Vegard's law) in Figure 1a,b. Second, the suitable or compatible electronegativity/polarizability between A^{n+} and B^{n+} is also the basic requirement, where we can reasonably design the range of B^{n+} concentration/proportion without phase separations. In fact, many cathode materials often share the same structural types in different rechargeable batteries as exhibited in Figure 1b,c. Furthermore, we can introduce B^{n+} with a higher electrode potential to enhance the average voltage of A-containing cathode materials. As shown in Figure 1c, Li$^+$ and K$^+$ give the higher electrode potential than that of Na$^+$ among the current ions secondary batteries, and importantly, those rechargeable batteries share the similar

"rocking chair" reaction mechanism based on ions insertion/extraction of electrode materials,[12] which potentially offers more opportunities to design high-voltage (>3.5 V) Na-ion cathode materials with respect to substitution and/or doping in the [A] sites. Herein, a K$^+$-modulated Na-ion cathode, $[K_{0.444(1)}Na_{1.414(1)}][Mn_{3/4}Fe_{5/4}](CN)_6$ as a proof of concept, has been prepared successfully based on the above discussion, which demonstrates a higher average voltage of ≈3.65 V versus Na$^+$/Na, superior cycling and structural stability.

2. Results and Discussion

Prussian blue analogs (PBAs), a large family of hexacyanoferrates, have attracted wide interests in rechargeable batteries owing to their open channel structure and abundant chemical

compositions.[13] Herein, K-based $K_{1.789}[Mn_{3/4}Fe_{5/4}](CN)_6 \cdot zH_2O$ ($z \approx 0.7$) compound with the Earth's abundant elements was used as a starting structural model from our previous study,[13c] for which K^+ presents a larger ionic radius of 1.38 Å (coordination number [CN] = 6) and higher electrode potential of –2.93 V than those of Na^+ in 1.02 Å and –2.71 V, respectively. Note that the general formula of PBA is $K_{1.789}[Mn_{3/4}Fe_{1/4}][Fe(CN)_6]$ for which we use $K_{1.789}[Mn_{3/4}Fe_{5/4}](CN)_6$ to be consistent with the proposed [A][TM][AG]. The basic information of this pristine material, including morphology, element distribution, crystal structure, and thermal stability, is shown in Figure S1–S4, Supporting Information. **Figure 2**a shows the charge–discharge curves of the $K_{1.789}[Mn_{3/4}Fe_{5/4}](CN)_6$ cathode in Na-based electrolyte with Na metal anode being cycled at a current density of 10 mA g^{-1} in the different voltage ranges. When first charged to 4.5 V, a capacity of about 160 mAh g^{-1} is delivered, which corresponds to almost all of K^+ extracted out of the pristine structure. However, only ≈1.6 mol Na^+ is inserted back to the host as discharged to 2.0 V with fresh electrolyte, resulting in a Coulombic efficiency of ≈88%; and the curves exhibit a big voltage drop at the beginning of discharge process, as well as a rapid attenuation after several cycles in Figure S5, Supporting Information. Four oxidation peaks at around 3.26, 3.65, 4.09, and 4.45 V are observed in the d(Q)/d(V) plots in Figure 2b and most of the capacity comes from the redox peaks at around 3.65 V. Therefore, an optimal cut-off voltage of 4.0 V is set to improve the reversibility, in which a highly reversible behavior with a capacity of ≈128 mAh g^{-1} is obtained corresponding to the similar oxidation process to the cut-off voltage of 4.5 V as shown in Figure 2b.

The X-ray diffraction (XRD) Rietveld refinement analysis combined with the inductively coupled plasma atomic emission

Table 1. Crystallographic and Rietveld refinement data of $K_{1.789}[Mn_{3/4}Fe_{5/4}](CN)_6$ cathode in the pristine state and after the first cycle.

	Pristine	After the first cycle
Composition	$K_{1.789}[Mn_{3/4}Fe_{5/4}](CN)_6$	$[K_{0.444(1)}Na_{1.414(1)}]$ $[Mn_{3/4}Fe_{5/4}](CN)_6$
Space group	P21/n—monoclinic	
Wavelengths	1.5406 Å	
Temperature	≈300 K	
Cell parameters	$a = 10.1222(6)$ Å	$a = 10.1489(19)$ Å
	$b = 7.2715(4)$ Å	$b = 7.2498(11)$ Å
	$c = 7.0299(5)$ Å	$c = 7.0721(11)$ Å
	$\alpha = \gamma = 90°$	$\alpha = \gamma = 90°$
	$\beta = 90.183(8)°$	$\beta = 90.288(17)°$
	$V = 517.42(6)$ Å^3	$V = 520.34(16)$ Å^3
Reliability factors	$R_{wp} = 6.73\%$	$R_{wp} = 3.94\%$
	$R_p = 5.28\%$	$R_p = 2.96\%$
	Gof = 1.785	Gof = 1.607
	$R_F^2 = 3.78\%$	$R_F^2 = 5.18\%$

spectrometry (ICP-AES) are performed to determine the structure and phase purity of $K_{1.789}[Mn_{3/4}Fe_{5/4}](CN)_6$ in the pristine state and its first cycle in 2.0–4.0 V versus Na^+/Na as shown in Figure 2c,d. The corresponding atomic coordinates, occupancies, and anisotropic displacement parameters (Å^2) are presented in Tables S1 and S2, Supporting Information. The results demonstrate that the two compounds share the same monoclinic structure with the space group of P21/n in **Table 1**, and the composition of the cycled compound is $[K_{0.444(1)}Na_{1.414(1)}][Mn_{3/4}Fe_{5/4}](CN)_6$. The cell volume is found
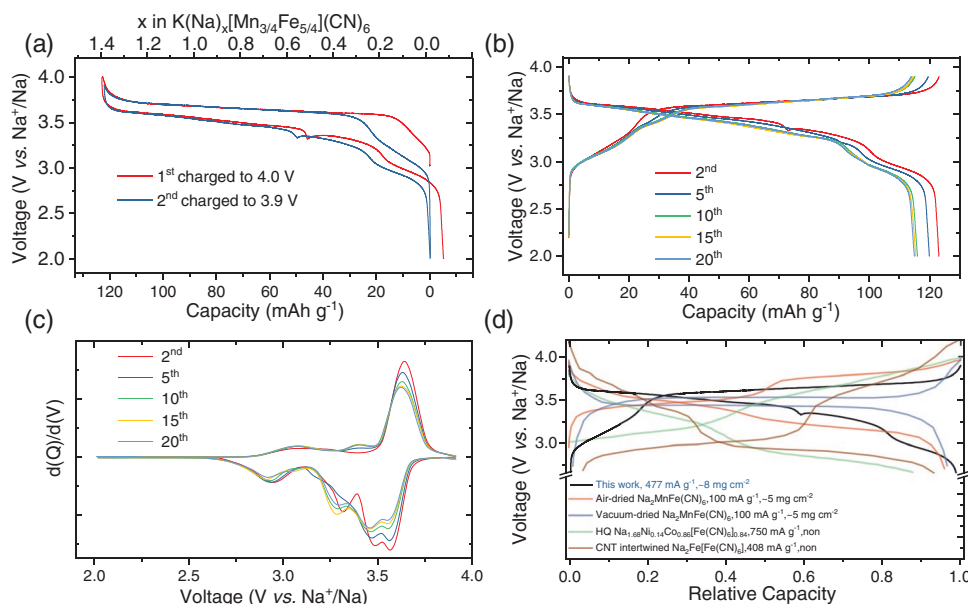
Figure 3. Tailoring the rational composition. a) Charge–discharge curves with the first cycle in the voltage range of 2.0–4.0 V and the second cycle in the voltage range of 2.0–3.9 V at a current density of 16 mA g^{-1} (corresponding to the rate of 0.1 C). b) Charge–discharge curves in the voltage range of 2.0–3.9 V at a current density of 20 mA g^{-1}. c) d(Q)/d(V) plots of the charge–discharge curves at different cycles. d) Comparison of the representative PBA Na-ion cathodes, including as-prepared K-stabilized $[K_{0.444(1)}Na_{1.414(1)}][Mn_{3/4}Fe_{5/4}](CN)_6$, air-dried $Na_2MnFe(CN)_6$,[18] high-crystallinity $Na_{1.68}Ni_{0.14}Co_{0.86}[Fe(CN)_6]_{0.84}$,[19] and CNT-intertwined $Na_2Fe[Fe(CN)_6]$.[17b]

to increase by 520.34(16) $Å^3$ against the 517.42(6) $Å^3$ before cycling, which can be owing to the additional Na^+ inserted in the host as shown in Figure 2a. The obtained crystal structure is displayed in Figure S6, Supporting Information, with Na/K disordered distributing in a typical open framework structure with N-coordinated $[Mn_{3/4}Fe_{1/4}]$ cations in 2d site and C-coordinated Fe cations in 2a site in agreement with the reports.[14] X-ray absorption near-edge spectroscopy (XANES) and Fourier transformed extended X-ray absorption fine structure (EXAFS) spectra further confirm that the oxidation states and local coordination environments of TMs have not been changed by the introduction of Na^+ as shown in Figure 2e–h.

Based on the above results, the electrochemical properties are further studied in following cycles. **Figure 3**a exhibits the charge–discharge curves at a current density of 16 mA g^{-1} (corresponding to the rate of 0.1 C), for which the different voltage ranges of the first cycle in 2.0–4.0 V and the second cycle in 2.0–3.9 V are set purposefully to leave a certain amount of Na^+ in the host. Therefore, the obtained cathode materials are recommended to be paired with Na-containing anode materials (e.g., Na-metal anodes[15] or the

presodiation hard carbon anodes[16]) to fabricate full cells. The corresponding d(Q)/d(V) plots show the very similar redox peaks in Figure S7, Supporting Information. The open circuit voltages of the sample measured by galvanostatic intermittent titration technique (GITT) with charging for 30 min at 16 mA g^{-1} and resting for 10 h during the first cycle in 2.0–4.0 V and the second cycle in 2.0–3.9 V further confirm the steadily thermodynamic process of bulk phase in Figure S7, Supporting Information. The charge–discharge curves and their d(Q)/d(V) plots in Figure 3c,d exhibit a highly reversible Na^+ extraction/insertion process in the following cycles, and about 93% capacity is retained after 100 cycles at the rate of 0.1 C in Figure S8, Supporting Information. The electrochemical impedance spectroscopy (EIS) measurements in Figure S9, Supporting Information, give a smaller impedance of around 38 Ω after 50 cycles, indicating the fast charge-transfer kinetics of Na^+ between the interface of electrolyte and the electrode material.[17] The results demonstrate that this in situ K^+-modulated host enables the highly electrochemical stability and reversible Na^+ extraction/insertion process. In addition, this cathode material
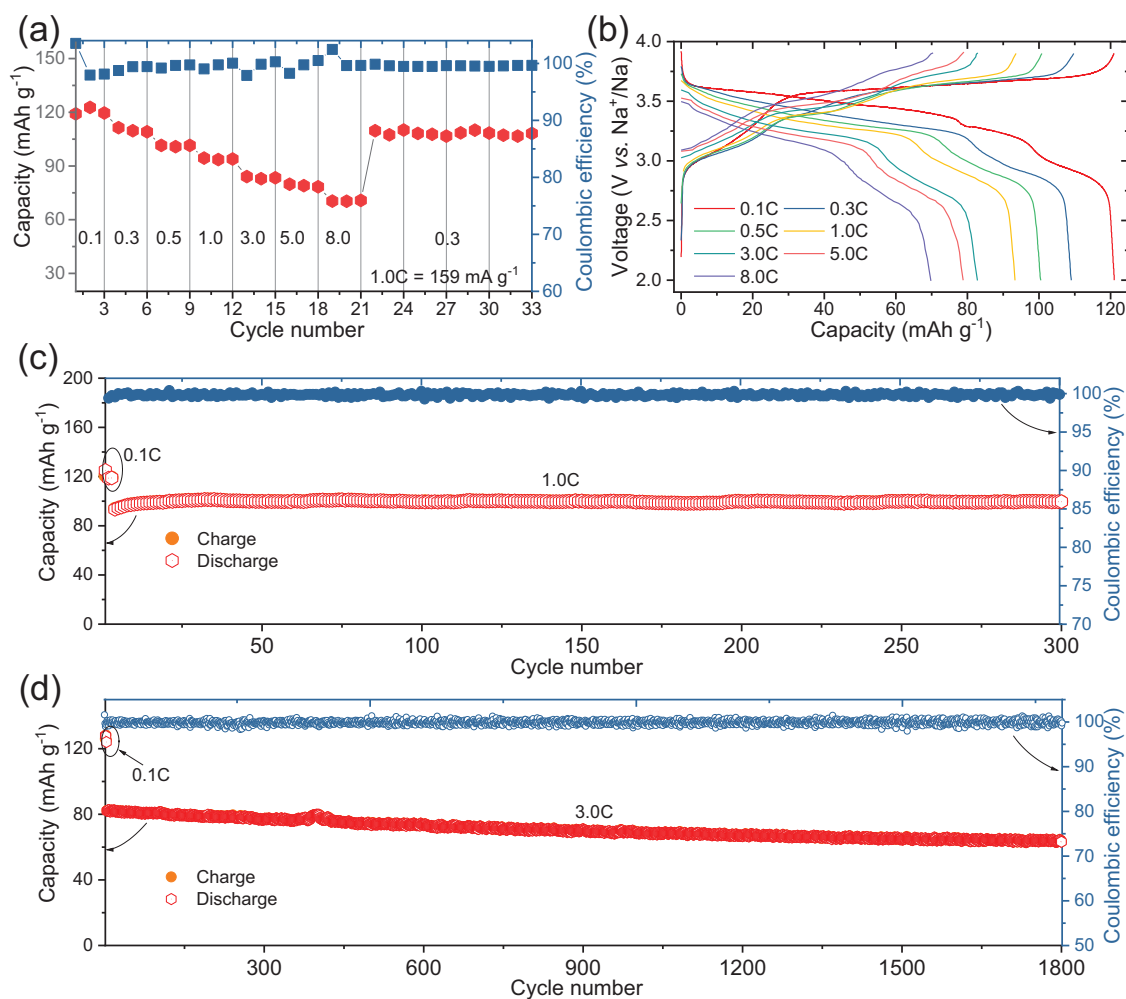
Figure 4. Electrochemical properties. a) Rate performance and b) the corresponding charge–discharge curves at a rate range of 0.1–8.0 C in the voltage range of 2.0–3.9 V. Long-term cycling performance at the rate density of c) 1.0 C and d) 3.0 C with the first three cycles at 0.1 C.

ADVANCED
SCIENCE NEWS
www.advancedsciencenews.com

ADVANCED
FUNCTIONAL
MATERIALS
www.afm-journal.de
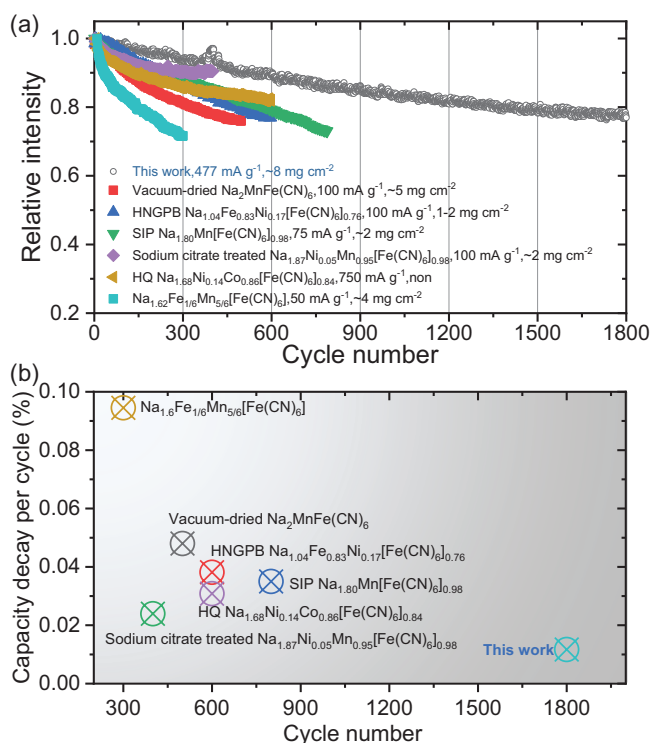
Figure 5. Comparison of long-term cycling performance on the representative Prussian blue analogs (PBA) Na-ion cathodes of a) capacity retention and b) capacity decay per cycle, including this present K-stabilized material, vacuum-dried $Na_2MnFe(CN)_6$,[18] high nickel gradient Prussian blue (HNGPB) $Na_{1.04}Fe_{0.83}Ni_{0.17}[Fe(CN)_6]_{0.76}$,[17a] small irregular particles (SIP) at size of 200–600 nm $Na_{1.80}Mn[Fe(CN)_6]$,[20] sodium citrate-treated $Na_{1.87}Ni_{0.05}Mn_{0.95}[Fe(CN)_6]_{0.98}$,[21] high-crystallinity $Na_{1.68}Ni_{0.14}Co_{0.86}[Fe(CN)_6]_{0.84}$,[19] and $Na_{1.6}Fe_{1/6}Mn_{5/6}[Fe(CN)_6]$.[22]

presents a higher average voltage of ≈3.65 V, directly contrasting the previous cathode materials of representative air-dried $Na_2MnFe(CN)_6$,[18] high-crystallinity $Na_{1.68}Ni_{0.14}Co_{0.86}[Fe(CN)_6]_{0.84}$,[19] and carbon nanotube (CNT) intertwined $Na_2Fe[Fe(CN)_6]$,[17b] as shown in Figure 3d.

The rate capability and long-term cycling stability are further tested to study the electrochemical properties of this material with the mass loading of the active material of ≈8 mg cm^{-2}. Rate performance and the corresponding charge–discharge curves at a rate range of 0.1–8 C in the voltage range of 2.0–3.9 V are shown in **Figure 4**a,b. The reversible capacities of about 121, 109, 101, 93, 83, 79, and 70 mAh g^{-1} are delivered at current rates of 0.1, 0.3, 0.5, 1.0, 3.0, 5.0, and 8.0 C, respectively, and after the rate cycling, a reversible capacity of about ≈110 mAh g^{-1} is achieved at 0.3 C in Figure 4a. The corresponding charge–discharge curves exhibit highly reversible behavior and small voltage hysteresis compared to the reported $Na_{2-x}[MnFe](CN)_6$.[13a,18] The long-term cycling stabilities at different rates of 1.0, 3.0, and 5.0 C are investigated as exhibited in Figure 4c,d and Figure S10, Supporting Information. A stable capacity retention with nearly 99% Coulombic efficiency is observed after 300 cycles at the rate of 1.0 C corresponding to the

current density of 159 mA g^{-1} as shown in Figure 4c. A long-term cycling stability at 3 C is obtained in Figure 4d, which exhibits the capacity retention of >78% over 1800 cycles with a much smaller capacity decay of ≈0.012% per cycle. The comparison of long-term cycling performance on the representative PBA Na-ion cathodes, including vacuum-dried $Na_2MnFe(CN)_6$,[18] high nickel gradient PB (HNGPB) $Na_{1.04}Fe_{0.83}Ni_{0.17}[Fe(CN)_6]_{0.76}$,[17a] small irregular particles at size of 200–600 nm $Na_{1.80}Mn[Fe(CN)_6]$,[20] sodium citrate-treated $Na_{1.87}Ni_{0.05}Mn_{0.95}[Fe(CN)_6]_{0.98}$,[21] high-crystallinity $Na_{1.68}Ni_{0.14}Co_{0.86}[Fe(CN)_6]_{0.84}$,[19] CNT-intertwined $Na_2Fe[Fe(CN)_6]$,[17b] and $Na_{1.6}Fe_{1/6}Mn_{5/6}[Fe(CN)_6]$,[22] are shown in **Figure 5**a,b indicating an ultra-stable capability of this present K-stabilized $[K_{0.444(1)}Na_{1.414(1)}][Mn_{3/4}Fe_{5/4}](CN)_6$ cathode material.

In order to further study the structural evolution of $[K_{0.444(1)}Na_{1.414(1)}][Mn_{3/4}Fe_{5/4}](CN)_6$ material in the long cycling process, the XRD analysis was performed at different states of charge of the 1st, 10th, 100th, and 300th cycles as shown in **Figure 6**. Rietveld refinement of corresponding XRD patterns is displayed in Figure 6a–c, which indicates that the as-prepared cathode material maintains a single phase during different cycles. The diffraction lines generally shift toward a low d space with the decreased cell volumes as the increase of the cycle numbers in Figure 6d,e. The corresponding crystallographic data, atomic coordinates, occupancies, and anisotropic displacement parameters (Å^2) are presented in Table S3–S8, Supporting Information. It is found that both the Na$^+$ and K$^+$ contents experience the decreasing trend upon increase; however, Na$^+$ decreases instantly from 1.414 to 1.344 mol as shown in Figure 6e. This suggests the capacity fading is mainly related to the irreversible Na$^+$ insertion. The morphology of the cathode before and after 100 cycles is collected in Figure S11, Supporting Information, in which no serious damage is observed. The energy dispersive spectrometry mappings of the cycled sample reveal a large amount of Na uniformly distributed on the particles, as well as the relatively small amount of K element. Importantly, the existence of K element is the bulk behavior, which is demonstrated by the X-ray photoelectron spectroscopy (XPS) of K 2p spectra at different depth profiles as shown in Figure S12, Supporting Information.

To further understand this design strategy, we investigate the K/Na mixing on the alkali sites in the PBA phase using the first-principles calculations based on the in-house code[23] by exploring geometrically distinct K/Na configurations on the shared sites of the $[K_xNa_{2-x}][Mn_{3/4}Fe_{5/4}](CN)_6$ structure at different K/Na ratios. We find that K/Na ions can mix on the alkali sites at a wide concentration range (0.5 < x < 2.0) close to the K side with multiple thermodynamically stable concentrations identified as shown in **Figure 7**a,b, indicating the feasibility of the construction of new material by electrochemical K-ion removal and resodiation. It is noteworthy that stable K/Na mixing can form at rather low K concentration (x < 0.5), which means that it is possible to realize the stabilization strategy with only a slight amount of alien (K) ion introduction. Sufficient amount of (Na) ions can remain to ensure the large capacity and high energy density of the substituted PBA.
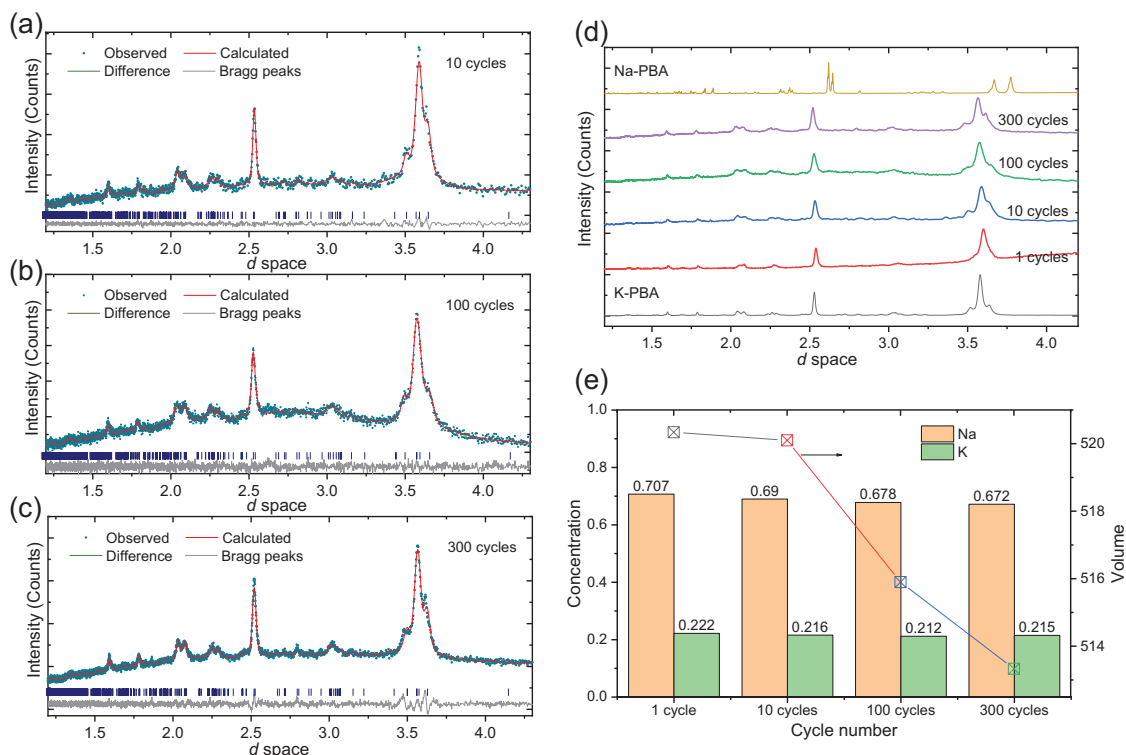
Figure 6. Structure analysis of the as-prepared cathode at different charge–discharge states and K/Na mixing in the alkali site in the $[K_xNa_{2-x}][Mn_{3/4}Fe_{5/4}]$ $(CN)_6$ host. Rietveld refinement of XRD patterns of $[K_{0.444(1)}Na_{1.414(1)}][Mn_{3/4}Fe_{5/4}](CN)_6$ at a) 10 cycles, b) 100 cycles, and c) 300 cycles. d) Comparison of the XRD patterns. e) The concentration of Na and K, and cell volume of the electrodes at different cycles.
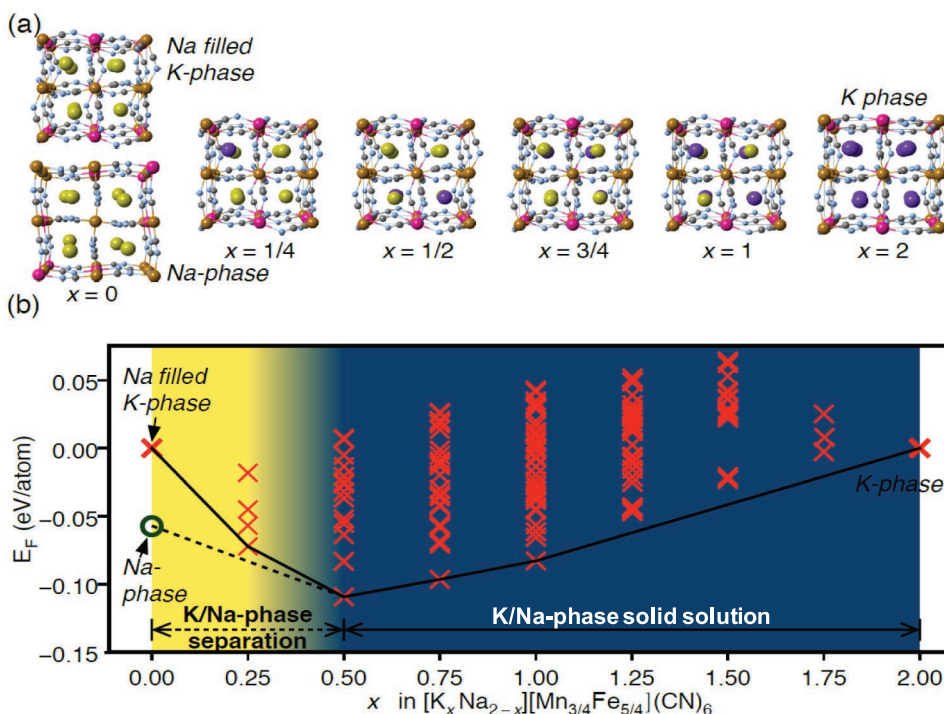
Figure 7. K/Na mixing in the alkali site in $[K_xNa_{2-x}][Mn_{3/4}Fe_{5/4}](CN)_6$ host. a) Thermodynamically stable K/Na mixing in the alkali sites at various concentrations. b) K/Na mixing convex hull. K/Na mixing can form at a wide concentration range $(0.5 < x < 2.0)$ with the K content can be no higher than 0.5 per formula unit. As a result, it is feasible to use a slight amount $(x < 0.5)$ of alien (K) ions to stabilize the whole alkali sublattice of the PBA compound.

3. Conclusions

In summary, we have proposed a promising approach by substitution in the alkali sites to prepare the high-performance and high-stability Na-ion cathode materials. This method provides a rational guidance on how to select and control the alien ions to achieve improved structural stability. As a proof of concept, a model material of $[K_{0.444(1)}Na_{1.414(1)}][Mn_{3/4}Fe_{5/4}](CN)_6$ is obtained based on the electrochemical reaction. This new cathode exhibits a higher average voltage of ≈ 3.65 V versus Na^+/Na and superior capacity retention of $>78\%$ after 1800 cycles with a much smaller capacity decay of $\approx 0.013\%$ per cycle. All the above results demonstrate that this in situ K^+-modulated host enables the high structural stability and reversible Na^+ extraction/insertion process. Compared to the general [TM]-site substitution, this study on the [A] sites provides more opportunities to develop new cathode materials of NIBs for improved properties.

4. Experimental Section

Materials Synthesis: $K_{1.789}[Mn_{3/4}Fe_{5/4}](CN)_6 \cdot xH_2O$ samples were prepared by a precipitation method. First, the stoichiometric precursors of $K_4Fe(CN)_6 \cdot 3H_2O$, $FeSO_4 \cdot 7H_2O$, and $MnSO_4 \cdot H_2O$ were directly mixed in saturated KCl solution under vigorous stirring at 60 °C for 12 h. After that, the as-prepared precipitates were separated by centrifugation and washed with deionized water. At last, the obtained samples were dried under vacuum at 100 °C for 12 h.

Materials Characterization: Powder XRD was performed using a Bruker D8 Advance diffractometer equipped with a Cu Kα radiation source ($\lambda_1 = 1.54060$ Å and $\lambda_2 = 1.54439$ Å) and a LynxEye_XE detector. Rietveld refinement of the XRD was carried out using the General Structure Analysis System software with the EXPGUI software interface.[24] The stoichiometry of the as-synthesized compound was determined measured by ICP-AES. The morphologies of the materials were investigated using a scanning electron microscope (Hitachi S-4800). High-resolution transmission electron microscopy images and scanning transmission electron microscopy (STEM) image and electron energy loss spectroscopy mappings were obtained using a 300 kV aberration-corrected (S)TEM (JEM-ARM300F, JEOL Ltd.) operated at 300 kV with a cold field-emission gun and double dodecapoles Cs correctors. Fourier transform infrared spectroscopy (Nicolet IS 50) was used to record the IR spectra of the sample in the range of 400–4000 cm. The XPS spectra were recorded with a spectrometer having Mg/Al K radiation (ESCALAB 250 Xi, Thermo Fisher). All binding energies reported were corrected using the signal of C at 284.4 eV as an internal standard. All samples were protected from air and moved to the detector cavity by the transfer equipment provided by Thermo Fisher. EIS measurements were carried out at room temperature using electrochemical S-4 impedance of IM6e (Zahner). Thermogravimetric analysis was conducted using a Diamond TG thermoanalyzer under a nitrogen atmosphere in a temperature range from room temperature to 500 °C at a heating rate of 10°C min^{-1}. X-ray absorption spectroscopy (XAS) spectra of the Fe K-edge and Mn K-edge were collected at P64 beamline (DESY, Hamburg, Germany). The transmission spectra were measured and monochromatized by a Si(111) double-crystal monochromator. The XANES spectra were processed by the Athena software package.[25]

Electrochemical Measurements: The working electrodes were prepared by mixing 80 wt% active material with 15 wt% acetylene black and 5 wt% polytetrafluoroethylene with the loading mass of the active material being ≈ 8 mg cm^{-2} in the size of 5×5 mm. The prepared electrodes were dried at 120 °C under vacuum for 12 h and then were fabricated into CR2032 coin-type cells with pure sodium foil as the counter electrode in an argon-filled glove box (H_2O, $O_2 < 0.1$ ppm).

A glass fiber was used as the separator, and 0.2 M $NaPF_6$ and 0.8 M $NaClO_4$ in ethylene carbonate/diethyl carbonate (EC/DEC = 4:6 in volume) with fluoroethylene carbonate (5% in volume) was used as the electrolyte. The charge and discharge measurements were carried out on a Land BT2000 battery test system (Wuhan, China) in voltage of various ranges under room temperature. GITT was measured by Maccor instrument by applying the repeated current pulses for 30 min followed by relaxation for 10 h. The relaxation time was set longer in order to achieve the equilibrium potential for the given electrode.

Computational Methods: All the DFT calculations reported in this study were conducted using the Vienna Ab initio Simulation Package[26] with projector augmented wave potentials. The exchange correlation was treated using the it is Perdew–Burke–Ernzerhof[26b] approach. For all calculations, a plane wave basis with a cut-off energy of 520 eV and Γ-centered k-meshes with a density of 8000 k-points per reciprocal atom was used.

Non-Equilibrium Phase Searching Method (NEPS): To explore the Na/K mixing in PBA phases, we created a $2 \times 2 \times 2$ supercell with eight alkali sites shared by Na and K ions and for each composition, we generated all the geometrically different configurations using NEPS.[23] All the configurations were then relaxed in DFT with the settings mentioned in the method section. The tendency of Na/K mixing on the alkali sites to form a mixed alkali metal PBA phase can be evaluated by computing the missing energy as shown in Equation (1)

$$E_{mix} = E(K_xNa_{2-x}Fe_{1.25}Mn_{0.75}(CN)_6) - \frac{x}{2}E(K_2Fe_{1.25}Mn_{0.75}(CN)_6) - (2-x)/2E(Na_2Fe_{1.25}Mn_{0.75}(CN)_6) \quad (1)$$

Where $E(K_xNa_{2-x}Fe_{1.25}Mn_{0.75}(CN)_6)$, $E(K_2Fe_{1.25}Mn_{0.75}(CN)_6)$, and $E(Na_2Fe_{1.25}Mn_{0.75}(CN)_6)$ are the total energies of the Na/K-mixed structure, original K-occupied structure, and Na fully replaced structure, respectively.

Supporting Information

Supporting Information is available from the Wiley Online Library or from the author.

Conflict of Interest

The authors declare no conflict of interest.

Keywords

[1]   a) Y. Li, Y. Lu, C. Zhao, Y.-S. Hu, M.-M. Titirici, H. Li, X. Huang, L. Chen, *Energy Storage Mater.* **2017**, *7*, 130; b) P. K. Nayak, L. Yang, W. Brehm, P. Adelhelm, *Angew. Chem., Int. Ed.* **2018**, *57*, 102.

[2]   a) W. Luo, F. Shen, C. Bommier, H. Zhu, X. Ji, L. Hu, *Accounts Chem. Res.* **2016**, *49*, 231; b) J.-Y. Hwang, S.-T. Myung, Y.-K. Sun, *Chem. Soc. Rev.* **2017**, *46*, 3529; c) J.-J. Kim, K. Yoon, I. Park, K. Kang, *Small Methods* **2017**, *1*, 1700219.

[3]   a) C. Zhao, Y. Lu, Y. Li, L. Jiang, X. Rong, Y.-S. Hu, H. Li, L. Chen, *Small Methods* **2017**, *1*, 1600063; b) H. Kim, H. Kim, Z. Ding, M. H. Lee, K. Lim, G. Yoon, K. Kang, *Adv. Energy Mater.* **2016**, *6*, 1600943; e) C. Zhao, Y. Lu, L. Chen, Y.-S. Hu, *Nano Res.* **2019**, *12*, 2018; f) C. Zhao, M. Avdeev, L. Chen, Y.-S. Hu, *Angew. Chem., Int. Ed.* **2018**, *57*, 7056.

[4]   a) Y. Sun, S. Guo, H. Zhou, *Energy Environ. Sci.* **2019**, *12*, 825; b) X. Rong, E. Hu, Y. Lu, F. Meng, C. Zhao, X. Wang, Q. Zhang, X. Yu, L. Gu, Y.-S. Hu, H. Li, X. Huang, X.-Q. Yang, C. Delmas, L. Chen, *Joule* **2019**, *3*, 503; c) H. Yu, Y. Ren, D. Xiao, S. Guo, Y. Zhu, Y. Qian, L. Gu, H. Zhou, *Angew. Chem., Int. Ed.* **2014**, *53*, 8963.

[5]   a) H. Kim, I. Park, S. Lee, H. Kim, K.-Y. Park, Y.-U. Park, H. Kim, J. Kim, H.-D. Lim, W.-S. Yoon, K. Kang, *Chem. Mater.* **2013**, *25*, 3614; b) B. Lee, D.-H. Seo, H.-D. Lim, I. Park, K.-Y. Park, J. Kim, K. Kang, *Chem. Mater.* **2014**, *26*, 1048.

[6]   a) Z. Jian, W. Han, X. Lu, H. Yang, Y.-S. Hu, J. Zhou, Z. Zhou, J. Li, W. Chen, D. Chen, L. Chen, *Adv. Energy Mater.* **2013**, *3*, 156; b) K. Kawai, W. Zhao, S.-I. Nishimura, A. Yamada, *ACS Appl. Energy Mater.* **2018**, *1*, 928; c) Y. Jiang, Z. Yang, W. Li, L. Zeng, F. Pan, M. Wang, X. Wei, G. Hu, L. Gu, Y. Yu, *Adv. Energy Mater.* **2015**, *5*, 1402104.

[7]   S. Lee, G. Kwon, K. Ku, K. Yoon, S.-K. Jung, H.-D. Lim, K. Kang, *Adv. Mater.* **2018**, *30*, 1704682.

[8]   P.-F. Wang, Y. You, Y.-X. Yin, Y.-S. Wang, L.-J. Wan, L. Gu, Y.-G. Guo, *Angew. Chem., Int. Ed.* **2016**, *55*, 7445.

[9]   a) Q. Wang, W. Yang, F. Kang, B. Li, *Energy Storage Mater.* **2018**, *14*, 361; b) C. Zhao, Q. Wang, Y. Lu, L. Jiang, L. Liu, X. Yu, L. Chen, B. Li, Y.-S. Hu, *Energy Storage Mater.* **2019**, *20*, 395; c) C. Zhao, Y. Lu, L. Chen, Y.-S. Hu, *InfoMat* **2019**, *2*, 126.

[10] K. Shiva, P. Singh, W. Zhou, J. B. Goodenough, *Energy Environ. Sci.* **2016**, *9*, 3103.

[11] a) S. C. Han, H. Lim, J. Jeong, D. Ahn, W. B. Park, K.-S. Sohn, M. Pyo, *J. Power Sources* **2015**, *277*, 9; b) Q. Zhu, H. Cheng, X. Zhang, L. He, L. Hu, J. Yang, Q. Chen, Z. Lu, *Electrochim. Acta* **2018**, *281*, 208; c) Q.-C. Wang, J.-K. Meng, X.-Y. Yue, Q.-Q. Qiu, Y. Song, X.-J. Wu, Z.-W. Fu, Y.-Y. Xia, Z. Shadike, J. Wu, X.-Q. Yang, Y.-N. Zhou, *J. Am. Chem. Soc.* **2019**, *141*, 840.

[12] M. M. Doeff, Y. Ma, S. J. Visco, L. C. De Jonghe, *J. Electrochem. Soc.* **1993**, *140*, L169.

[13] a) L. Wang, Y. Lu, J. Liu, M. Xu, J. Cheng, D. Zhang, J. B. Goodenough, *Angew. Chem., Int. Ed.* **2013**, *52*, 1964; b) Y. Lu, L. Wang, J. Cheng, J. B. Goodenough, *Chem. Commun.* **2012**, *48*, 6544; c) L. Jiang, Y. Lu, C. Zhao, L. Liu, J. Zhang, Q. Zhang, X. Shen, J. Zhao, X. Yu, H. Li, X. Huang, L. Chen, Y.-S. Hu, *Nat. Energy* **2019**, *4*, 495.

[14] L. Xue, Y. Li, H. Gao, W. Zhou, X. Lü, W. Kaveevivitchai, A. Manthiram, J. B. Goodenough, *J. Am. Chem. Soc.* **2017**, *139*, 2164.

[15] a) H. Yadegari, X. Sun, *Accounts Chem. Res.* **2018**, *51*, 1532; b) C. Zhao, Y. Lu, J. Yue, D. Pan, Y. Qi, Y.-S. Hu, L. Chen, *J. Energy Chem.* **2018**, *27*, 1584; c) Q. Shi, Y. Zhong, M. Wu, H. Wang, H. Wang, *Angew. Chem., Int. Ed.* **2018**, *57*, 9069; d) H. Wang, C. Wang, E. Matios, W. Li, *Angew. Chem., Int. Ed.* **2018**, *57*, 7734; e) Q. Wang, C. Zhao, X. Lv, Y. Lu, K. Lin, S. Zhang, F. Kang, Y.-S. Hu, B. Li, *J. Mater. Chem. A* **2019**, *7*, 24857.

[16] a) J. Liu, Z. Yang, J. Wang, L. Gu, J. Maier, Y. Yu, *Nano Energy* **2015**, *16*, 389; b) B. Zhang, R. Dugas, G. Rousse, P. Rozier, A. M. Abakumov, J.-M. Tarascon, *Nat. Commun.* **2016**, *7*, 10308.

[17] a) B. Wang, Y. Han, Y. Chen, Y. Xu, H. Pan, W. Sun, S. Liu, M. Yan, Y. Jiang, *J. Mater. Chem. A* **2018**, *6*, 8947; b) Y. You, H.-R. Yao, S. Xin, Y.-X. Yin, T.-T. Zuo, C.-P. Yang, Y.-G. Guo, Y. Cui, L.-J. Wan, J. B. Goodenough, *Adv. Mater.* **2016**, *28*, 7243; c) Q. Zhang, L. Fu, J. Luan, X. Huang, Y. Tang, H. Xie, H. Wang, *J. Power Sources* **2018**, *395*, 305.

[18] J. Song, L. Wang, Y. Lu, J. Liu, B. Guo, P. Xiao, J.-J. Lee, X.-Q. Yang, G. Henkelman, J. B. Goodenough, *J. Am. Chem. Soc.* **2015**, *137*, 2658.

[19] J. Peng, J. Wang, H. Yi, W. Hu, Y. Yu, J. Yin, Y. Shen, Y. Liu, J. Luo, Y. Xu, P. Wei, Y. Li, Y. Jin, Y. Ding, L. Miao, J. Jiang, J. Han, Y. Huang, *Adv. Energy Mater.* **2018**, *8*, 1702856.

[20] Z. Shen, S. Guo, C. Liu, Y. Sun, Z. Chen, J. Tu, S. Liu, J. Cheng, J. Xie, G. Cao, X. Zhao, *ACS Sustainable Chem. Eng.* **2018**, *6*, 16121.

[21] R. Chen, Y. Huang, M. Xie, Z. Wang, Y. Ye, L. Li, F. Wu, *ACS Appl. Mater. Interfaces* **2016**, *8*, 31669.

[22] W. Li, C. Han, W. Wang, Q. Xia, S. Chou, Q. Gu, B. Johannessen, H. Liu, S. Dou, *Adv. Energy Mater.* **2020**, *10*, 1903006.

[23] a) Z. Yao, S. Kim, J. He, V. I. Hegde, C. Wolverton, *Sci. Adv.* **2018**, *4*, eaao6754; b) Z. Yao, S. Kim, M. Aykol, Q. Li, J. Wu, J. He, C. Wolverton, *Chem. Mater.* **2017**, *29*, 9011.

[24] S. C. Vogel, *J. Appl. Cryst.* **2011**, *44*, 873.

[25] B. Ravel, M. Newville, *J. Synchrotron Radiat.* **2005**, *12*, 537.

[26] a) G. Kresse, J. Hafner, *Phys. Rev. B* **1993**, *47*, 558; b) J. P. Perdew, M. Ernzerhof, K. Burke, *J. Chem. Phy.* **1996**, *105*, 9982; c) G. Kresse, J. Fursthmüller, *Phys. Rev. B* **1996**, *54*, 11169.